



Article

The Performance of Fibrous CDC Electrodes in Aqueous and Non-Aqueous Electrolytes

Siret Malmberg^{1,2,*} , Mati Arulepp², Krista Laanemets¹, Maike Käärik³, Ann Laheäär², Elvira Tarasova¹, Viktoria Vassiljeva¹, Illia Krasnou¹ and Andres Krumme¹ 

¹ Department of Materials and Environmental Technology, Tallinn University of Technology, Ehitajate tee 5, 19086 Tallinn, Estonia; krista.laanemets@gmail.com (K.L.); elvira.tarasova@ttu.ee (E.T.); viktoria.vassiljeva@ttu.ee (V.V.); illia.krasnou@taltech.ee (I.K.); andres.krumme@taltech.ee (A.K.)

² Skeleton Technologies OÜ, Valukoja 8, 11415 Tallinn, Estonia; mati.arulepp@skeletontech.com (M.A.); ann.laheaar@skeletontech.com (A.L.)

³ Institute of Chemistry, University of Tartu, Ravila 14a, 50411 Tartu, Estonia; maike.kaarik@ut.ee

* Correspondence: siret.malmberg@taltech.com

Abstract: The aim of this study was to investigate the electrochemical behaviour of aqueous electrolytes on thin-layer (20 μm) nanoporous carbide-derived carbon (CDC) composite fibrous directly electrospun electrodes without further carbonisation. There have been previously investigated fibrous electrodes, which are produced by applying different post-treatment processes, however this makes the production of fibrous electrodes more expensive, complex and time consuming. Furthermore, in the present study high specific capacitance was achieved with directly electrospun nanoporous CDC-based fibrous electrodes in different neutral aqueous electrolytes. The benefit of fibrous electrodes is the advanced mechanical properties compared to the existing commercial electrode technologies based on pressure-rolled or slurry-cast powder mix electrodes. Such improved mechanical properties are preferred in more demanding applications, such as in the space industry. Electrospinning technology also allows for larger electrode production capacities without increased production costs. In addition to the influence of aqueous electrolyte chemical composition, the salt concentration effects and cycle stability with respect to organic electrolytes are investigated. Cyclic voltammetry (CV) measurements on electrospun electrodes showed the highest capacitance for asymmetrical cells with an aqueous 1 M $\text{NaNO}_3\text{-H}_2\text{O}$ electrolyte. High CV capacitance was correlated with constant current charge–discharge (CC) data, for which a specific capacitance of 191 F g^{-1} for the positively charged electrode and 311 F g^{-1} for the negatively charged electrode was achieved. The investigation of electrolyte salt concentration on fibrous electrodes revealed the typical capacitance dependence on ionic conductivity with a peak capacitance at medium concentration levels. The cycle-life measurements of selected two-electrode test cells with aqueous and non-aqueous electrolytes revealed good stability of the electrospun electrodes.

Keywords: electrospun electrode; EDL capacitance; carbide-derived carbon; supercapacitor; aqueous electrolytes



Citation: Malmberg, S.; Arulepp, M.; Laanemets, K.; Käärik, M.; Laheäär, A.; Tarasova, E.; Vassiljeva, V.; Krasnou, I.; Krumme, A. The Performance of Fibrous CDC Electrodes in Aqueous and Non-Aqueous Electrolytes. *C* **2021**, *7*, 46. <https://doi.org/10.3390/c7020046>

Academic Editor: Bruno C. Janegitz

Received: 19 April 2021

Accepted: 12 May 2021

Published: 14 May 2021

Publisher's Note: MDPI stays neutral with regard to jurisdictional claims in published maps and institutional affiliations.



Copyright: © 2021 by the authors. Licensee MDPI, Basel, Switzerland. This article is an open access article distributed under the terms and conditions of the Creative Commons Attribution (CC BY) license (<https://creativecommons.org/licenses/by/4.0/>).

1. Introduction

With the need to decrease CO_2 emissions, enormous effort has been put into the development of electrochemical energy storage devices such as batteries, fuel cells, and supercapacitors, supporting the shift to more extensive incorporation of renewable energy sources. Supercapacitors, also called electrical double layer capacitors (EDLCs), are energy storage devices with high power density and long cycle stability [1–3]. From the application requirements perspective, supercapacitors bridge the gap between lithium-ion batteries and electrolytic capacitors [4]. EDLCs are mostly attractive for further development due to their possible use as load levelling devices in renewable energy technology [5] and to further enhance electrical vehicle performance [6–8].

The energy storage mechanism of supercapacitors relies on the electrochemical double layer (EDL), which forms between the electrode material and the electrolyte [9–11]. Liquid electrolytes can typically be classified as non-aqueous, aqueous and ionic liquids (ILs) [12]. In general, the requirements for an ideal electrolyte are high ionic conductivity, chemical and electrochemical stability (wide potential window), wide operating temperature range, low volatility and flammability, environmental friendliness, and feasible cost at scale [13]. However, in real applications, few of the parameters often need to be compromised. The specific performance of an EDL depends on the interactions between the carbon with a high surface area and the electrolyte ions [4,14–16]. Therefore, it is important that the properties of the electrolyte meet the demands from the pore structure of the carbon.

The effect of various aqueous electrolytes has been extensively studied with various carbon powder composite electrodes [17–19]. A few studies have been performed with fibrous electrodes [20] or electrospun carbon-containing electrodes [21] in aqueous electrolytes but, to our knowledge, no studies have directly electrospun fibrous electrodes of CDCs. The most fundamental studies have been performed with $\text{H}_2\text{SO}_4\text{-H}_2\text{O}$ and $\text{KOH-H}_2\text{O}$ electrolytes, but these electrolytes are corrosive and have a working voltage range up to 1.0 V [22–24]. Therefore, neutral aqueous solutions such as $\text{Li}_2\text{SO}_4\text{-H}_2\text{O}$, $\text{Na}_2\text{SO}_4\text{-H}_2\text{O}$ and $\text{K}_2\text{SO}_4\text{-H}_2\text{O}$ are preferred to avoid the harmful effects of acidic and alkaline environments [22]. Furthermore, the activated carbons were tested for operating voltages up to 1.6 V in symmetrical cells of aqueous $\text{Na}_2\text{SO}_4\text{-H}_2\text{O}$ and long-term stability (<10,000 cycles) [22,25].

To achieve high EDL capacitance, the size of the electrolyte ions must correspond to the pore size of carbon [26]. Cai et al. showed the effects of anions and cations with graphene-based nanocomposite electrodes, where 0.5 M aqueous solutions of sodium salts displayed a specific capacity of the SO_4^{2-} anion that was 21% higher than that of the NO_3^- anions [27]. In monovalent cation electrolytes, the specific capacitance increases under the influence of the corresponding cationic radius. In common aqueous electrolyte solutions, the ionic radii of cations decrease as follows: $\text{Li}^+ > \text{Na}^+ > \text{K}^+$ (0.69, 1.2 and 1.5 Å, respectively) [27–29].

Electrospinning is a versatile fibre forming process for generating ultra-fine fibres from different materials, such as polymers, ceramics and composites [30]. Electrospun fibres can be used in many applications, such as filtering materials [31,32], sensors [33] or energy storage [34]. In the case of energy storage, electrospun fibrous electrodes have been mainly used with a combination of post-treatment processes [35,36] or with a multi-step electrospinning method [37]. The benefit of directly electrospun nanofibres is the simplicity of the process, as it does not include any post-treatment methods, such as pyrolysis and thermal treatment. Such post-treatments have been proven to be effective in eliminating the negative performance impacts of the relatively high content of non-capacitive polymer in the spun layer matrix, which is necessary for efficient fibre formation [37,38]. However, the carbonisation process itself is destructive to the fibrous structure, which in turn decreases the mechanical durability and certainly has a relatively high cost impact from a large-scale production point of view.

Our research group has previously shown that the advanced mechanical durability and flexibility of electrospun electrodes is related to their fibrous structure [38]. Furthermore, despite the relatively high polymer content, the capacitance per carbon contained remains almost constant compared to tape-casted and rolled pressed (PTFE) technologies [39].

In our previous work, electrospun carbide-derived carbon (CDC) nanofibre electrodes were studied with a focus on non-aqueous electrolytes, out of which the best performance was achieved in combination with 1.5 M spiro-(1,1′)-bipyrrrolidinium tetrafluoroborate in acetonitrile (SBP- $\text{BF}_4\text{-ACN}$), with a potential window of 3.0 V and gravimetric capacitance of 95.3 F g^{-1} and 78.5 F g^{-1} for positively and negatively charged electrodes, respectively [39,40]. The advantages of applying non-aqueous electrolytes are a wider operative temperature range and wide potential stability range, leading to a higher energy density than aqueous electrolytes [4,12,26,41,42]. Thus, the major drawback of aqueous electrolytes

is the lower operative voltage, which is limited by the water decomposition voltage of 1.23 V [4,12,43–45]. However, the benefit of using aqueous electrolytes comes from low cost [45,46], environmental friendliness, [13,41] and higher ionic conductivity [13], leading to low resistance and superior power performance [3,41,44].

Therefore, goal of this study is to investigate the effect of aqueous electrolytes on the EDL capacitance, resistance and cyclability of electrospun fibrous CDC-based electrodes. The specific effects of cations and anions in aqueous solutions are evaluated in a three-electrode system configuration, and the cycle-life performance of both aqueous and non-aqueous electrolytes is studied in two-electrode systems.

The stability during charge–discharge cycling of post-treated fibrous electrodes in aqueous media has been tested by Stojanovska et al., where stable performance was achieved for more than 1000 cycles [47]. Furthermore, T. He et al. showed good cycle stability and a high capacitance retention of ~99.3% after 1000 cycles of polyacrylonitrile/polyvinyl-pyrrolidone electrospun composite fibres in an IL-based electrolyte in 1-butyl-3-methylimidazolium hexafluorophosphate [36]. Compared to fibrous electrodes, activated carbon-based cast electrodes have also shown long and stable cycle stability in aqueous and non-aqueous electrolytes [25,48,49]. In addition, L. Demarconnay et al. showed stable cycle stability up to 10,000 cycles at different voltage limits with cast electrodes in a 0.5 M aqueous Na₂SO₄-H₂O system [25]. However, the effect of different electrolytes on the cycle-life performance of directly electrospun electrodes has not been studied to our knowledge.

2. Experimental Section

2.1. Materials and Processes

The electrodes for electrochemical analysis of cation and anion influence on EDL performance in aqueous electrolytes were prepared by the electrospinning method, according to a similar electrode process and recipe from our previous studies [39,40]. The carbide-derived carbon active material was purchased from Skeleton Technologies OÜ (Tallinn, Estonia). Titanium carbide was converted to porous CDC carbon by applying Cl₂ treatment at 900 °C. A hydrogen gas purification step at 800 °C was applied to remove residues of chlorine in the converted CDC. The CDC material initial particle size was 1–5 µm, which was further milled to reduce the size of particles to ~100 nanometres. The detailed milling procedure is described in our previous work [40] and more detailed carbon surface chemistry is discussed by M. Käärik et al. [15] The resulting milled CDC particles were mixed with a carbon conductive additive (Super C, Timcal, Deutschland GmbH, Düsseldorf, Germany) at a ratio of 80/20 (wt %). The carbon mixture was sonicated in dimethylformamide (DMF, Sigma Aldrich, Tartu, Estonia) for 2 h. After sonication, mechanical stirring was applied for another 24 h at 40 °C, after which polyacrylonitrile (PAN, Sigma Aldrich, Tartu, Estonia M_w = 150,000 g mol⁻¹) was added to the solution at 7% weight, and the solution was stirred for an additional 24 h at 40 °C. The weight ratio of polymer to total mass of carbon was 50/50 in the solution. Finally, 15% by weight of 1-ethyl-3-methylimidazolium tetrafluoroborate (EMIm-BF₄, Sigma Aldrich, Tartu, Estonia, purity ≥ 99.9%) ionic liquid (IL) was added to the electrospinning solution and stirred for 0.5 h before the electrospinning process was initiated. The addition of IL is necessary to increase the conductivity of the solution for a stable electrospinning process. The electrospinning parameters were set as constant: solution pumping rate of 0.5 mL h⁻¹, applied DC voltage of 15 kV, and a distance between spinneret and rotating drum of 8 cm. After electrospinning, the fibrous electrodes were mechanically compressed by a hydraulic static press (Scamia) to achieve better electrical contacts between the fibres. The morphology of the CDC-based fibrous electrode was evaluated by scanning electron microscopy (SEM, Gemini Zeiss Ultra 55, Graz, Austria), as shown in Figure 1.

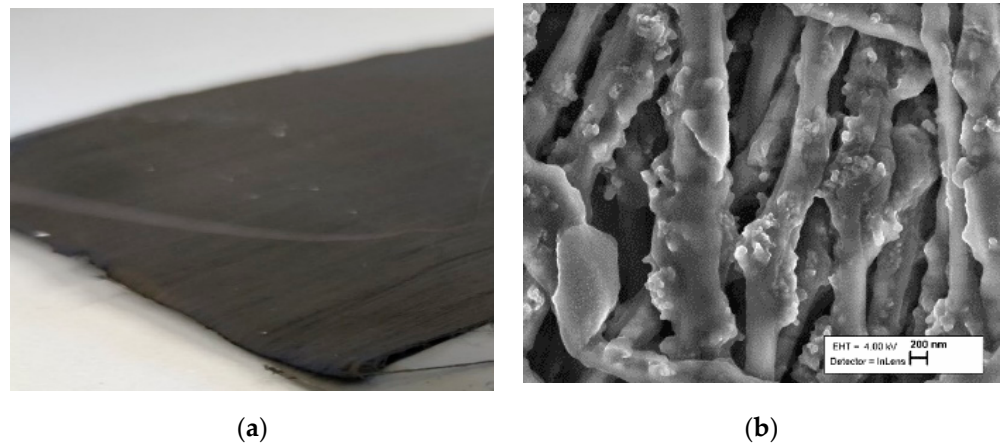


Figure 1. (a) Electrospun electrode $3 \times 4 \text{ cm}^2$ sheet and (b) morphology of the fibres by examined SEM.

The porosity characteristics of the CDC powder before and after milling and of the electrospun electrode were determined from the N_2 adsorption method at $-196 \text{ }^\circ\text{C}$ using the NOVA touch LX2 (Quantachrome Instruments, Boynton Beach, FL, USA). Before gas adsorption measurement, the carbon samples were dried for 12 h under a vacuum at $300 \text{ }^\circ\text{C}$, and the electrode sample was dried at $100 \text{ }^\circ\text{C}$ to avoid strongly exceeding the glass transition temperature of PAN. The Brunauer–Emmett–Teller surface area (S_{BET}) was calculated from N_2 adsorption data according to BET theory [50] at a pressure interval P/P_0 of 0.02–0.2, and the total pore volume (V_{tot}) was calculated at a P/P_0 of 0.97. Calculations of the pore size distribution (PSD), micropore volume (V_μ) and specific surface area (S_{dft}) were performed by using the quenched solid density functional theory (QSDFT) equilibria model for slit-type pores. The N_2 adsorption–desorption isotherms are shown in Figure 2, and the porosity characteristics are presented in Table 1. The isotherms of CDCs appear as Type I, corresponding to microporous materials [51]. One can see from the porosity analysis that both the specific surface area of carbon and the amount of micropores slightly decreased during the milling process.

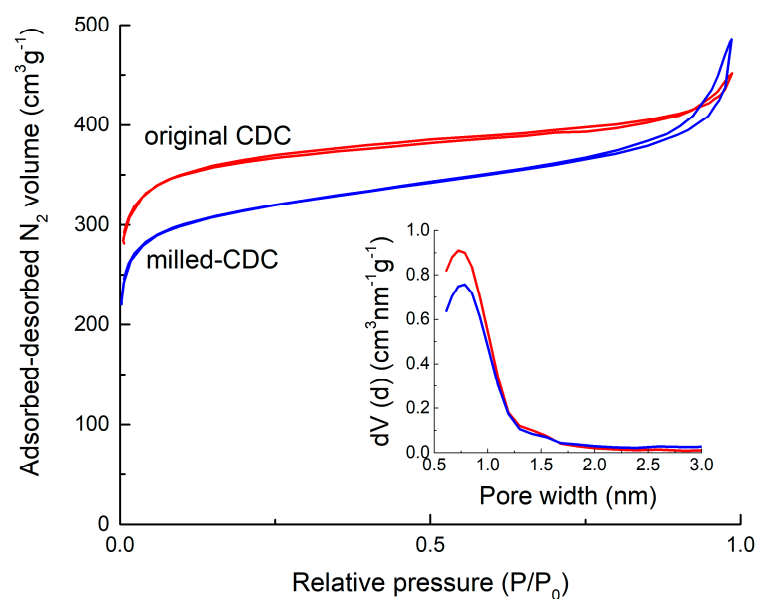


Figure 2. N_2 absorption–desorption isotherms and pore size distribution of the CDC before and after milling.

Table 1. Porosity characteristics of CDC.

Material	S_{ABET} $m^2 g^{-2}$	S_{dft} $m^2 g^{-2}$	V_{tot} $cm^3 g^{-2}$	$V_{\mu dft}$ $cm^3 g^{-2}$
Non-milled	1282	1390	0.67	0.53
Milled	1098	1173	0.66	0.44

The thermal stability of the electrode was evaluated by thermal gravimetric analysis (Labsys EVO TG DTA 1600 °C, Ankara, Turkey). The temperature increase rate was set to 5 °C min⁻¹, and the sample was heated to 600 °C. The start of degradation of the electrode was observed at ~250 °C.

The mechanical properties of the electrospun CDC-based fibrous electrodes were evaluated by an Instron 5866 (Norwood, MA, USA) tensile testing machine. For optimal mechanical properties, morphology, and capacitance (tested after the stress test), a specific stress of 2.32×10^{-4} N TEX⁻¹ was determined. More detailed porosity analysis, TGA and mechanical strength analysis can be found in our previous works [38–40].

The intermolecular interactions within the nanofibrous mats treated with Na₂SO₄-H₂O, NaNO₃-H₂O and KNO₃-H₂O aqueous electrolytes were analysed by Fourier transform infrared spectroscopy (FTIR). FTIR spectra obtained by means of Interspec 200-X (Tartu, Estonia) instrument with attenuated total reflection (ATR) unit. A wavenumber range a 400–4000 cm⁻¹ with a 0.5 cm⁻¹ resolution was used. IR absorption spectra show significant stability of electrospun PAN fibres in electrolytes and strong absorption of anions on the fibre surface. The measured FTIR spectra are presented in Figure 3. To analyse the influence of electrolytes on the intermolecular interactions of PAN/DMF fibres, electrospun samples were kept in the electrolytes for 48 h and thereafter washed with distilled water to remove the salt residues. Afterwards, the samples were dried under a vacuum at 95 °C for 24 h. The reference data in Figure 3 show the peaks of pure electrospun PAN fibre. Bands attributed to main chain groups, C-C stretching vibrations (1245 cm⁻¹), C-H symmetric vibrations (2936 cm⁻¹ and 1360 cm⁻¹), and in- and out-of-plane bending vibrations (1450 cm⁻¹ and 1071 cm⁻¹, respectively), demonstrate neither polymer decomposition nor macromolecular structure changes after exposure to the electrolyte [52–55]. The most common PAN undergoes hydrolysis and thermal oxidation in the dissolved state. However, no corresponding peaks were observed. Furthermore, the absorption band of the nitrile side group (C≡N, 2245 cm⁻¹) shows no significant change in intensity or peak area, which means no hydrogen bond formation between the nitrogen atom of the nitrile group and anions, NO₃⁻ or SO₄²⁻, was observed. At the same time, peaks corresponding to the above-mentioned anions were present in the spectra of PAN electrodes exposed to the electrolyte. For nitrate-based electrolytes, a strong peak at 1356 cm⁻¹ and a small peak at 835 cm⁻¹ were observed, corresponding to asymmetric and symmetric stretching of the NO₃⁻ group, respectively [53]. For the sulphate-based electrolyte, the peaks were located at 1123 cm⁻¹ and 615 cm⁻¹, indicating asymmetric stretching of SO₄²⁻ groups [54]. This can be explained by the absorption of salt anions via electrostatic interactions with dipoles formed on the fibre surface by the -C≡N group of PAN [56]. Thus, one could conclude the chemical stability of electrospun fibres in the studied electrolytes together with the ability to absorb anions on the fibre surface.

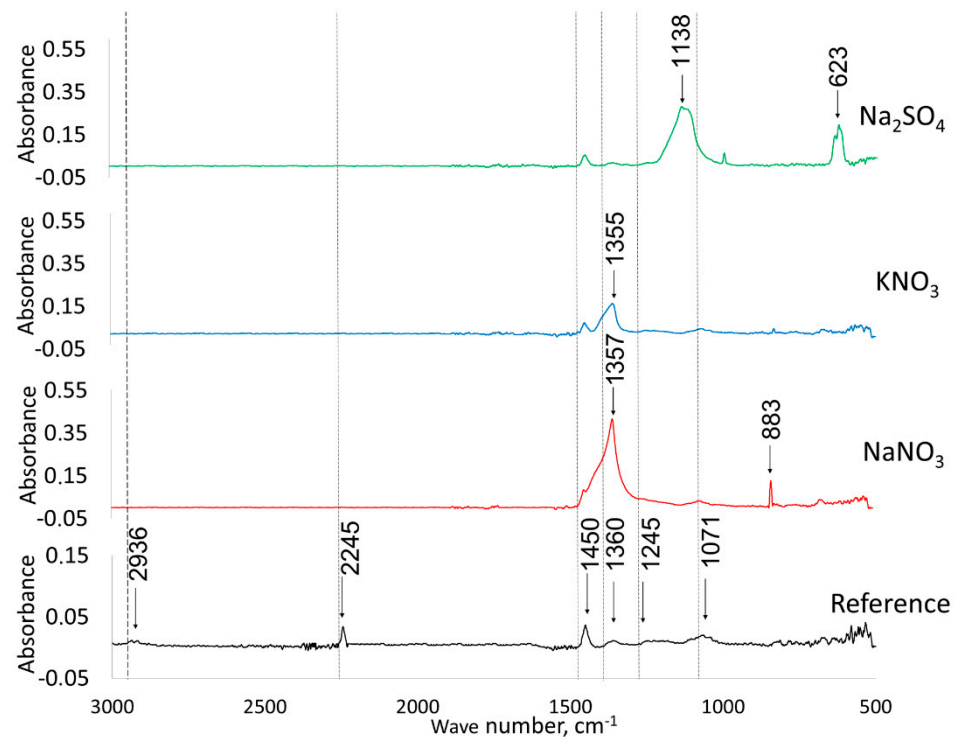


Figure 3. FTIR spectra of PAN/DMF fibre (reference) and the fibres soaked in aqueous 1.0 M electrolytes: $\text{Na}_2\text{SO}_4\text{-H}_2\text{O}$, $\text{KNO}_3\text{-H}_2\text{O}$, $\text{KNO}_3\text{-H}_2\text{O}$.

Two- and three-electrode test cells were used for electrochemical testing. Electrospun fibrous mats with a coating weight of 1.86 g m^{-2} were used in all experimental cells. A working electrode (WE) with a diameter of 6 mm was cut for the 3-electrode cells, and identical electrodes of 15 mm diameter were cut for the 2-electrode set-up. For 3-electrode systems, a 15 mm diameter counter electrode (CE) and $\text{Ag} | \text{AgCl}$ (3.5 M KCl) reference electrode (RE) were used. Prior to cell assembly, the cut electrodes were dried in a vacuum oven at $100 \text{ }^\circ\text{C}$ for 24 h. The electrodes were then contacted with gold current collectors in electrochemical test cells. The WE and CE were interleaved by a 1 mm thick glass fibre separator membrane (purchased from VWR, Dresden, Germany). The 2-electrode test cells applied a cellulosic separator (purchased Nippon Kodoshi, Kochi, Japan).

Three aqueous electrolyte solutions from different salts— $\text{NaNO}_3\text{-H}_2\text{O}$ (Lach-Ner, Neratovice, Czech Republic), $\text{KNO}_3\text{-H}_2\text{O}$ (Sigma-Aldrich, Tartu, Estonia) and $\text{Na}_2\text{SO}_4\text{-H}_2\text{O}$ (Sigma-Aldrich, Tartu, Estonia)—were prepared to study the EDLC of CDC-based electrospun fibrous electrodes. For the analysis of the electrolyte ionic composition effect, the concentration of the electrolyte solutions was kept constant at 1.0 M. To additionally investigate the effect of electrolyte concentration on the capacitance and resistance, the NaNO_3 -based electrolyte concentration was altered from 0.2 M to 5.0 M. The electrolyte conductivity was measured at room temperature with a Benchtop conductivity metre (SevenCompactTM S230, Columbus, OH, USA). Electrolyte pH was measured by a standard $\text{Ag} | \text{AgCl}$ double junction pH combination electrode (Sigma-Aldrich, Tartu, Estonia). The physical parameters of the selected salts and electrolyte solutions are presented in Table 2.

Table 2. Conductivity, pH values and ion sizes [30] for used aqueous electrolytes.

Salt	Molarity, M	Conductivity, mS cm ⁻¹	pH	Ion Radius, nm	
				Cation	Anion
Na ₂ SO ₄	1.0	78.2	7.13	0.12	0.24
KNO ₃	1.0	73.2	7.34	0.15	0.17
NaNO ₃	0.2	73.0	6.85		
NaNO ₃	1.0	89.2	7.10		
NaNO ₃	2.5	103.0	7.08	0.12	0.17
NaNO ₃	5.0	117.2	7.02		

The 3-electrode studies were conducted with all electrolyte alternatives, while 2-electrode stability studies were performed with two aqueous and two organic electrolytes: 1 M NaNO₃-H₂O, 1 M KNO₃-H₂O, and 1.5 M 1-ethyl-3-methylimidazolium-bis (trifluoromethyl sulfonyl) imide in acetonitrile (EMIm-TFSI-ACN) and SBP-BF₄-ACN. The selection of aqueous electrolytes for cycle life analysis was based on the results of 3-electrode cells. The choice of organic electrolytes was made based on the results of our previous work, where the maximum potential window of $dU \leq 3.5$ V was determined in 1.5 M EMIm-TFSI-ACN, showing an identical gravimetric capacitance of 89.8 F g⁻¹ for positively and negatively charged electrodes. Second, the largest potential window of 3.0 V was reached in 1.5 M SBP-BF₄-ACN-type quaternary ammonium salt-based electrolytes, with a gravimetric capacitance of 95.3 F g⁻¹ and 78.5 F g⁻¹ for positively and negatively charged electrodes, respectively [16].

2.2. Electrochemical Evaluation Methods

Cyclic voltammetry (CV), constant current cycling (CC) and electrochemical impedance spectroscopy (EIS) tests were performed to electrochemically evaluate the electrospun fibrous electrodes. All electrochemical measurements were performed at room temperature with Gamry Interface 1010 E equipment (Warminster, PA, USA).

CV plots were obtained from 3-electrode measurements in the potential range of +0.6 V to -0.7 V (vs. Ag|AgCl RE) at potential scan rates of 200 to 5 mV s⁻¹. The capacitance was calculated by dividing the measured current i by the applied potential scan rate v , according to Equation (1):

$$C = \frac{i}{v} \quad (1)$$

A constant current charge–discharge study was performed between the potential limits of +0.6 V to 0 V and -0.6 V to 0 V for positively and negatively charged electrodes, respectively, (vs. Ag|AgCl RE). The experiments were performed with different polarisation potentials to determine the DL- properties of the cation and anion of different electrolytes. To achieve the maximum capacitance limits for positively and negatively charged electrodes, the cells were held at fixed potential for 5 min and then discharged; thereafter, the next cycle was started as shown in Figure 4.

Similar charge–discharge profiles were repeated five times in both positive and negative potential regions. EDL capacitance values were counted from the last three cycles. The current density was varied between 0.1 and 2 mA cm⁻². The capacitance values for positively (C_+) and negatively (C_-) charged electrodes were calculated by integrating the discharge curves according to Equation (2):

$$\begin{aligned} C_+ &= \int_{0.6}^0 \frac{|I|dt}{\Delta E} \\ C_- &= \int_{-0.6}^0 \frac{|I|dt}{\Delta E} \end{aligned} \quad (2)$$

where I is the current density, dt is the discharge time, and ΔE is the potential range of the positively or negatively charged electrodes (0.6 V) [42].

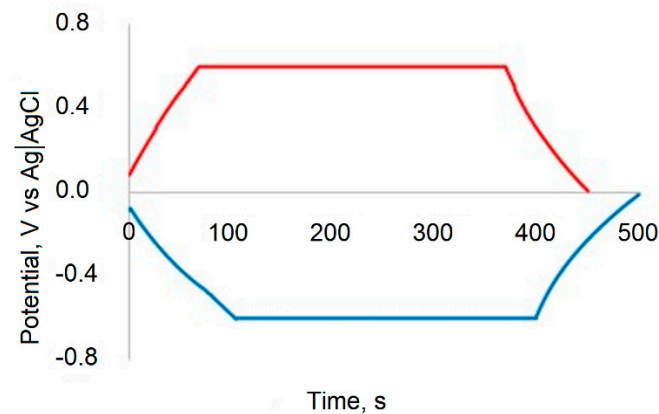


Figure 4. Constant current discharge curve at 0.25 mA cm^{-2} .

The EIS spectra were measured in the AC frequency range from 1 MHz to 50 mHz at an amplitude of the sinusoidal voltage of 5 mV. The total impedance (Z) of RC circuits was described by Equation (3):

$$Z = Z' + Z'' = R + \frac{1}{j\omega C_s} \quad (3)$$

where Z' is described as the real impedance, Z'' is the imaginary impedance, j is the imaginary number $\sqrt{-1}$, ω is the angular frequency $\omega = 2\pi f$, and C_s is the series capacitance.

R_s values were determined by frequency response analysis and are equal to real impedance, $R_s = Z'$.

The series capacitance C_s values of the EIS were calculated from Equation (4) [57,58]:

$$C_s = -\frac{1}{\omega Z''} \quad (4)$$

The specific capacitance values were obtained by dividing the capacitance value from different methods by the mass of carbon in the working electrode.

The CV method was used to evaluate the cycle stability of electrospun electrodes in various organic and aqueous electrolytes in a two-electrode test cell configuration. The cycling test was performed at a potential scan rate of $v = 20 \text{ mV s}^{-1}$ for <3000 cycles. The applied voltage range for organic electrolytes was 0 to 2.3 V and, for the aqueous electrolytes, the voltage limit was reduced to 1.0 V to prevent water decomposition. The capacitance decrease was monitored via the CV method, while the resistance (R_s) increase was evaluated by the EIS method at 0 V (DC), at $f = 1 \text{ kHz}$.

3. Results and Discussion

3.1. Electrochemical Evaluation of Fibrous Electrodes in Aqueous Electrolytes

The stability and ideal polarisation region of fibrous CDC-based electrodes in the selected aqueous electrolytes was evaluated by cyclic voltammetry [59], for which three-electrode cell curves are as shown in Figure 5.

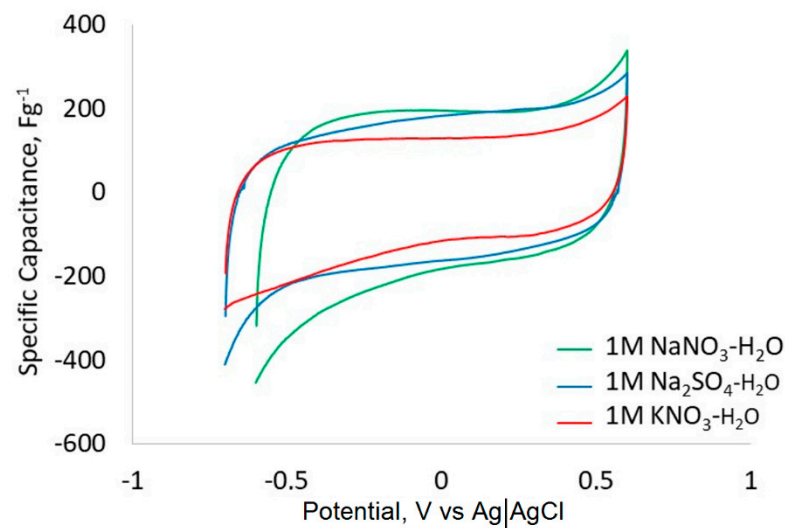


Figure 5. Cyclic voltammograms expressed as capacitance per CDC weight in fibrous electrodes in 1 M aqueous electrolytes ($v = 20 \text{ mV s}^{-1}$).

Aqueous electrolyte solutions are known to cause reduction reactions at higher negative electrode potentials, leading to the formation of hydrogen gas and water oxidation reactions at the positive electrode potential limits, resulting in the formation of oxygen. In the case of the $\text{KNO}_3\text{-H}_2\text{O}$ electrolyte, the oxidation and reduction processes are somewhat less evident in Figure 5, as the potential limits have not yet been reached or exceeded significantly. When the cation is replaced from K^+ to Na^+ , an exponential increase in current at potentials close to -0.5 V was observed, indicating the possible competing hydrogen ion adsorption and reduction on the carbon surface in parallel with adsorption of Na^+ , being more pronounced compared to the K^+ based electrolyte. Furthermore, differences in the capacitance of nitrate-based electrolytes were observed for both positive and negative electrode potential regions, being lower for the KNO_3 electrolyte. This can be explained by the different cation sizes of Na^+/K^+ , and during such measurements, cation and anion adsorption are still slightly affected by the reduction and oxidation processes. According to the CV curves presented in Figure 5, no difference in capacitance was observed in the positively charged region by the exchange of anions from NO_3^- to SO_4^{2-} , although the nitrate ion was much smaller than the sulphate ion. To further study the ion-related capacitance effects, the CC method was applied at current densities between 0.1 and 2 mA cm^{-2} , with the results presented in Figure 6a–c and in Table 3.

Table 3. Gravimetric capacitance values for positively and negatively charged electrodes evaluated by CC tests at a current density of 0.5 mA cm^{-2} in 1 M solutions.

Electrolyte	C^+ Electrode, F g^{-1}	C^+ CDC, F g^{-1}	C^- Electrode, F g^{-1}	C^- CDC, F g^{-1}
$\text{NaNO}_3\text{-H}_2\text{O}$	40.8	177.5	63.5	276.1
$\text{KNO}_3\text{-H}_2\text{O}$	47.7	132.0	57.0	157.6
$\text{Na}_2\text{SO}_4\text{-H}_2\text{O}$	34.6	150.7	51.0	221.9

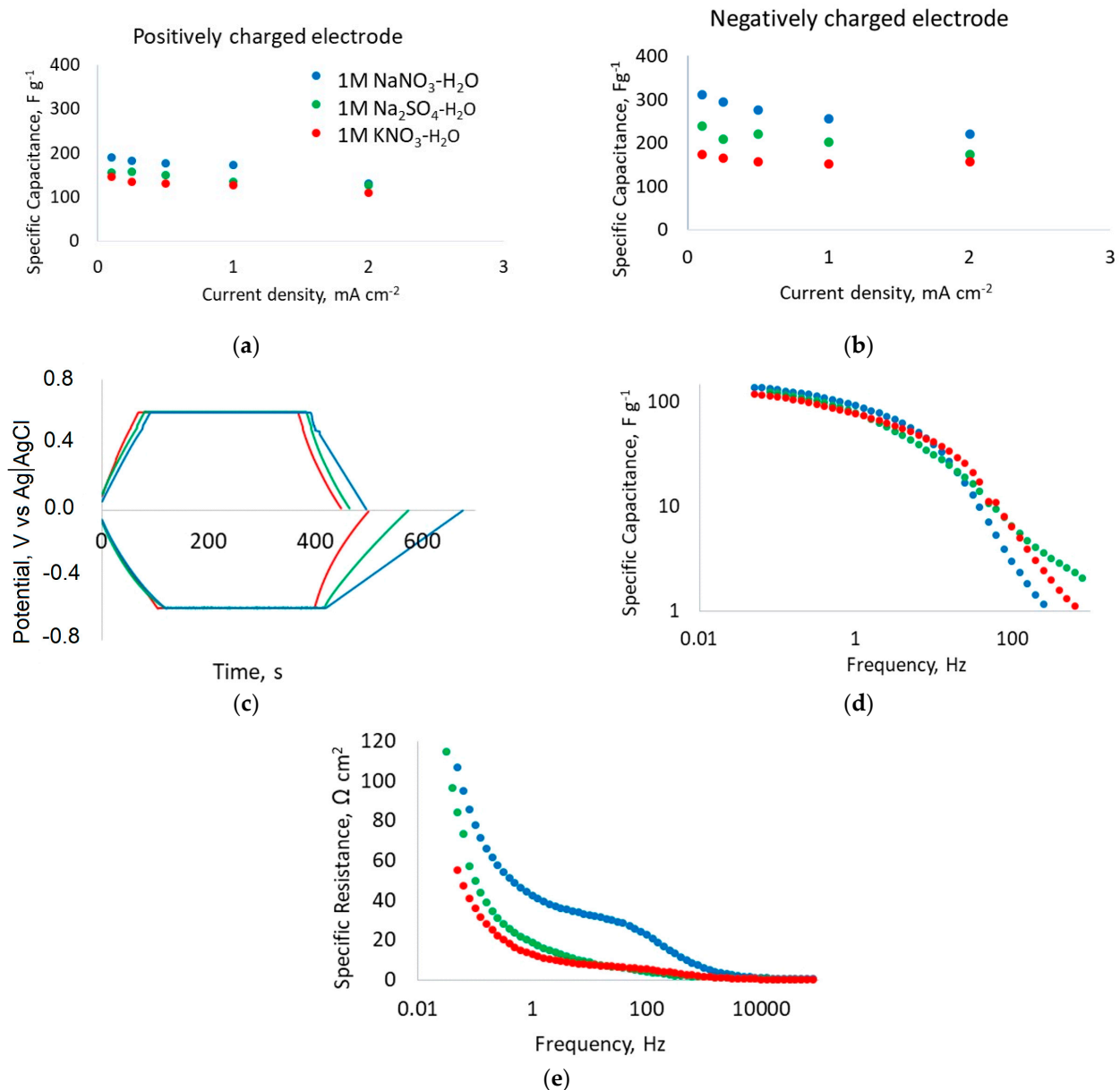


Figure 6. Electrochemical performance of “electropsun” CDC based fibrous electrodes in aqueous electrolytes: (a,b) specific capacitance values from CC discharge plots at $I = 0.5 mA cm^{-2}$ for positively and negatively charged electrodes, (c) CC charge–discharge, curves $I = 0.5 mA cm^{-2}$ (d) specific capacitance, C_s as a function of frequency and (e) resistance, R_s as a function of frequency from EIS measurements at 0 V vs. Ag|AgCl.

The capacitance dependence of the negatively charged electrode (Figure 6b) shows that Na^+ , with an ion size 20% smaller than the K^+ ion, increases the specific capacitance up to 30% at a current density of $2 mA cm^{-2}$. By reducing the applied current density, the ions have a longer time to migrate and adsorb onto the carbon surface and, thus, the specific capacitance increases even more. When the NO_3^- anion was replaced by SO_4^{2-} , the specific capacitance at $2 mA cm^{-2}$ was practically equal, although the ion radius of the SO_4^{2-} anions was significantly larger than that of NO_3^- (Figure 6a). This result is in line with the previously described CV measurements. However, by reducing the applied current density, the specific capacitance in $NaNO_3-H_2O$ increased compared to SO_4^{2-} , as expected according to the ion size comparison.

The effect of the aqueous electrolytes on the capacitance and resistance of fibrous CDC-based electrodes was further evaluated by electrochemical impedance spectroscopy

measurements recorded at DC = 0 V (vs. ref) to characterise the uncharged surface properties. Based on these measurements, the series capacitance values were calculated using Equation (4), and the results are shown in Figure 6d. In all three studied electrolyte solutions, the adsorption of ions into carbon pores begins at frequencies $f < 100$ Hz, with a steep increase in capacitance. At $f < 1$ Hz, a capacitance plateau begins to form when most ions are adsorbed to carbon micropores (Figure 6d). The capacitance in different 1.0 M solutions did not differ significantly, which can be explained by the uncharged ($E_{DC} = 0$ V) electrode surface. In the frequency range of 10–100 kHz, much lower R_s values were obtained compared to the low-frequency ranges (Figure 6e) due to electrolyte ion migration and adsorption/desorption rate effects, i.e., At high frequency, ions do not have enough time to migrate to the carbon pores, and the electrode behaves like a smooth surface. Ion adsorption reaches maximum levels only at low frequencies, which is reflected by the significant increase in capacitance and resistance [2,40]. Surprisingly, the highest resistance was observed in the low frequency region of the $\text{NaNO}_3\text{-H}_2\text{O}$ solution, although it has the smallest anion/cation size and slightly higher conductivity compared to other electrolytes.

3.2. Effect of Electrolyte Concentration on Fibrous Electrode Performance

The effect of electrolyte salt concentration on the electrochemical performance of fibrous CDC-based electrodes was evaluated in $\text{NaNO}_3\text{-H}_2\text{O}$ solutions of 0.2 M, 1.0 M, 2.5 M, and 5.0 M molarity. The conductivity and pH values of the prepared electrolytes are shown in Table 1. The specific capacitance of positively and negatively charged electrodes was determined at different current densities of CC, presented in Figure 7a,b. The areal capacitance as a function of frequency and Nyquist plots are presented in Figure 7c,d, respectively.

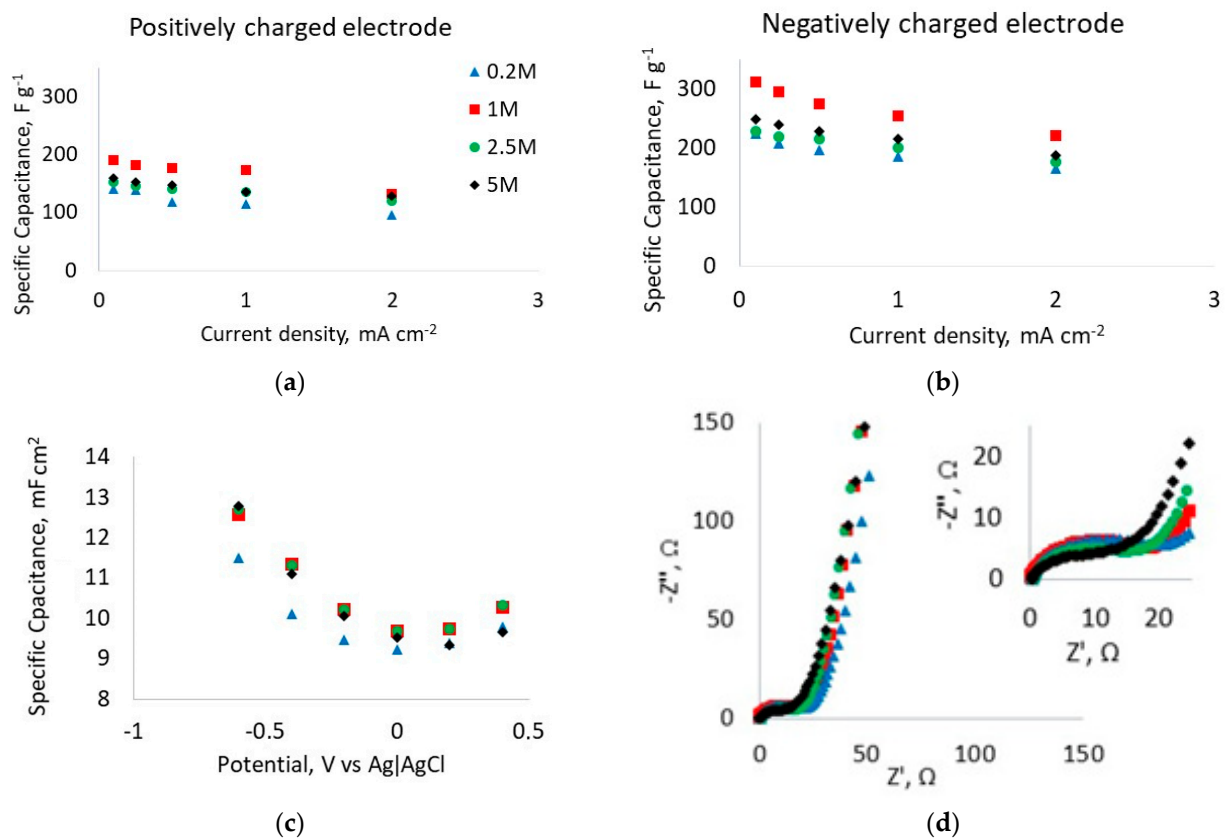


Figure 7. Electrochemical performance of “electropsun” CDC-based fibrous electrodes in xM NaNO_3 electrolytes: (a,b) capacitance values obtained from CC discharge plots at $I = 0.5 \text{ mA cm}^{-2}$ for positively and negatively charged electrodes, (c) C_s (at $I = 50 \text{ mHz}$) as a function of potential from EIS measurements and (d) Nyquist plot at 0 V (vs. Ag|AgCl).

The rate capability analysis (C vs. I in Figure 7a,b) gave the highest capacitance at a concentration of 1.0 M of NaNO_3 . However, it is generally known that by increasing the concentration of electrolyte salt, the charge-transfer resistance of EDLC cells is decreased while the capacitance and rate capability are increased [60,61]. However, there are no major differences in the obtained capacitance values, as higher salt concentrations also increase the viscosity of the electrolyte and promote the saturation of active ions on the carbon surface [60,61].

The capacitance-potential dependency was additionally analysed with the EIS method at different fixed electrode potentials (Figure 7c). It was confirmed that negatively charged electrodes have higher capacitance over the electrode area, as also observed by the CC measurements. The change in capacitance as a function of the electrode potential is precisely defined, where it has a clear minimum for all solution concentrations close to zero charge potential of 0 V vs. $\text{Ag} | \text{AgCl}$, with marginal effects from the concentration. Some differences in the absolute capacitance values from CC and EIS measurements are mainly due to the differences in the measurement methodology. The capacitance from the EIS technique is calculated at relatively high frequencies (~ 50 mHz) at which the boundary diffusion of different electrolyte ions has not yet been reached, while constant current measurements at very low current densities of 0.1 mA cm^{-2} allow for the finite ion diffusion to occur.

The Nyquist plots (Figure 7d) show the highest impedance for the cells with the lowest ionic conductivity electrolyte of 0.2 M concentration. Figure 7d also shows a small decrease in charge-transfer resistance (semi-circle) for uncharged electrodes by increasing the salt concentration. Additionally, the differences in capacitance and resistance decreased at higher concentrations because enough electrolyte ions were adsorbed on the carbon electrode. However, due to the increase in viscosity at higher concentrations, the expected increase in capacitance and decrease in resistance were less evident. Such results are well in accordance with the CC measurement data.

3.3. Cycle-Stability Analysis for Full Cells

Two-electrode systems were applied to analyse the long-term cycle stability of fibrous CDC-based electrode materials. Cycle-life tests in selected aqueous and non-aqueous electrolytes were performed using the CV method ($v = 20 \text{ mVs}^{-1}$) in voltage ranges of 0–1.0 V and 0–2.3 V, respectively, where the change in capacitance was assessed during CV discharge cycles, and the change in resistance was evaluated by EIS at $f = 1 \text{ kHz}$. The capacitance and resistance change over the cycles is shown in Figure 8a,b. Stable results over ~ 1000 cycles were observed for both aqueous electrolytes and the organic 1.5 M $\text{SBP-BF}_4\text{-ACN}$ electrolyte. An exponential decrease in capacitance and increase in resistance during cycling was observed in the 1.5 M EMIm-TFSI-ACN electrolyte. Such unstable behaviour can be caused by the relatively high viscosity of the electrolyte and possibly an excessively high voltage scanning rate, which does not support efficient ion transfer and adsorption on the electrodes [40]. For the $\text{SBP-BF}_4\text{-ACN}$ and $\text{KNO}_3\text{-H}_2\text{O}$ electrolytes, no significant change in capacitance was observed over the cycles. The increase in $\text{SBP-BF}_4\text{-ACN}$ cell resistance was typical of EDL capacitors and increased by only 21% over 3000 cycles, while the resistance of the KNO_3 capacitor was almost constant.

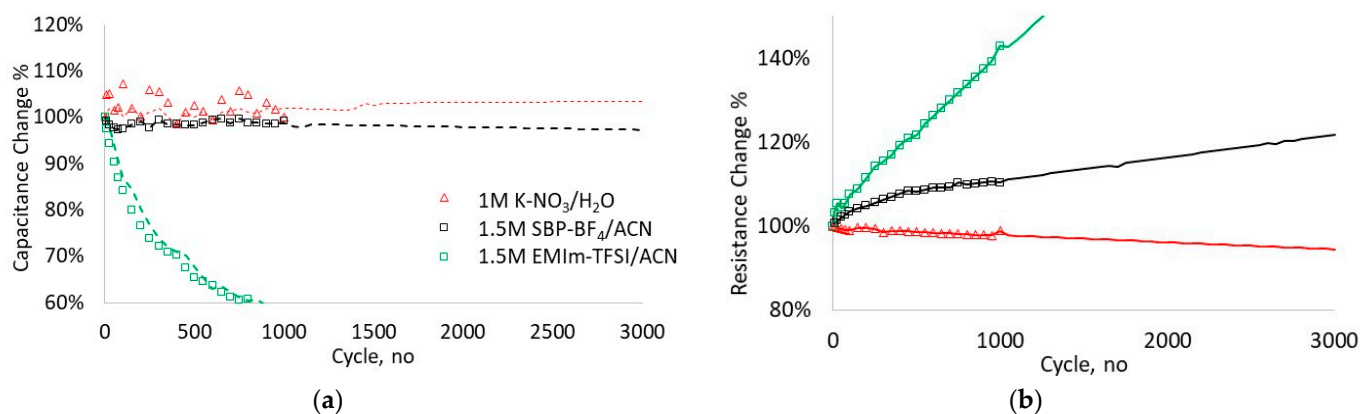


Figure 8. Cycle-life performance of fibrous CDC-based electrodes of 1000 cycles (shapes) with extrapolation of 3000 cycles (lines): (a) capacitance retention by CV at 20 mV s^{-1} and (b) series resistance change during cycling by EIS.

4. Conclusions

The present study investigated the influence of aqueous $\text{NaNO}_3\text{-H}_2\text{O}$, $\text{KNO}_3\text{-H}_2\text{O}$ and $\text{Na}_2\text{SO}_4\text{-H}_2\text{O}$ electrolyte ionic composition and concentration on the electrochemical behaviour of directly electrospun carbide-derived carbon electrodes. The highest gravimetric capacitances of 191 F g^{-1} and 311 F g^{-1} for positively and negatively charged electrodes, respectively, were achieved in $1 \text{ M NaNO}_3\text{-H}_2\text{O}$ at 0.1 mA cm^{-2} . The capacitance values in $1 \text{ M Na}_2\text{SO}_4\text{-H}_2\text{O}$ and $1 \text{ M KNO}_3\text{-H}_2\text{O}$ electrolyte solutions were 23% and 30% lower than that of $\text{NaNO}_3\text{-H}_2\text{O}$, respectively. The results correlate well with the electrolyte ion sizes.

A salt concentration effect study on the fibrous electrodes showed that a $\text{NaNO}_3\text{-H}_2\text{O}$ concentration of 1.0 M is optimum for capacitive performance. On the other hand, a higher salt concentration ($>1 \text{ M}$) slightly improved the cell resistance at the expense of increased electrolyte conductivity.

Based on the analysis of the two-electrode cells, a stable cycle life was achieved with both non-aqueous $\text{SBP-BF}_4\text{-ACN}$ and aqueous $\text{NaNO}_3\text{-H}_2\text{O}$ and $\text{Na}_2\text{SO}_4\text{-H}_2\text{O}$ electrolytes. In the case of aqueous electrolyte solutions, some further ion absorption effects were observed in the first few hundred cycles of the cycle-life test, leading to an increase in capacitance, followed by a generally expected declining trend.

Author Contributions: Data curation, S.M., K.L., M.K.; investigation, S.M., K.L., M.K. and E.T.; methodology, S.M. and M.A.; resources, V.V.; supervision, M.A. and A.K.; validation, S.M., K.L., M.K. and I.K.; writing—original draft, S.M.; writing—review and editing, A.K., M.A. and A.L. All authors have read and agreed to the published version of the manuscript.

Funding: This work was financially supported by the European Space Agency, ESA contract number 4000119258/16/NL/CBi “Fully electrospun durable electrode and electrochemical double-layer capacitor for high frequency applications” and the European Union European Regional Development Fund through Foundation Archimedes (TK143).

Institutional Review Board Statement: Not applicable.

Acknowledgments: We thank senior researcher Valdek Mikli for SEM analyses and Can Rüstü Yörük for TGA analyses.

Conflicts of Interest: The authors declare no conflict of interest.

References

1. Yu, A.; Chabot, V.; Zhang, J. *Electrochemical Supercapacitors for Energy Storage and Delivery: Fundamentals and Applications*; CRC Press: Boca Raton, FL, USA, 2017.
2. Beguin, F.; Frackowiak, E. *Supercapacitors: Materials, Systems, and Applications*; John Wiley & Sons: Hoboken, NJ, USA, 2013.
3. Zhong, C.; Deng, Y.; Hu, W.; Qiao, J.; Zhang, L.; Zhang, J. A review of electrolyte materials and compositions for electrochemical supercapacitors. *Chem. Soc. Rev.* **2015**, *44*, 7484–7539. [[CrossRef](#)]

4. Menzel, J.; Fic, K.; Frackowiak, E. Hybrid aqueous capacitors with improved energy/power performance. *Prog. Nat. Sci. Mater. Int.* **2015**, *25*, 642–649. [[CrossRef](#)]
5. Guerrero-Martínez, M.Á.; Romero-Cadaval, E.; Minambres-Marcos, V.; Milanés-Montero, M.I. Supercapacitor Energy Storage System for Improving the Power flow in Photovoltaic Plants. *Electron. Compon. Mater.* **2014**, *44*, 3. [[CrossRef](#)]
6. Zhao, C.; Zheng, W. A Review for Aqueous Electrochemical Supercapacitors. *Front. Energy Res.* **2015**, *3*, 1–5. [[CrossRef](#)]
7. Horn, M.; MacLeod, J.; Liu, M.; Webb, J.; Motta, N. Supercapacitors: A new source of power for electric cars? *Econ. Anal. Policy* **2019**, *61*, 93–103. [[CrossRef](#)]
8. Burke, A.; Zhao, H. *Applications of Supercapacitors in Electric and Hybrid Vehicles*; 5th European Symposium on Supercapacitor and Hybrid Solutions (ESSCAP): Brasov, Romania, 2015; p. 15.
9. Weingarh, D.; Noh, H.; Foelske-Schmitz, A.; Wokaun, A.; Kötz, R. A reliable determination method of stability limits for electrochemical double layer capacitors. *Electrochim. Acta* **2013**, *103*, 119–124. [[CrossRef](#)]
10. Käärik, M.; Arulepp, M.; Käärik, M.; Maran, U.; Leis, J. Characterization and prediction of double-layer capacitance of nanoporous carbon materials using the Quantitative nano-Structure-Property Relationship approach based on experimentally determined porosity descriptors. *Carbon* **2020**, *158*, 494–504. [[CrossRef](#)]
11. Arulepp, M.; Leis, J.; Lätt, M.; Miller, F.; Rumma, K.; Lust, E.; Burke, A. The advanced carbide-derived carbon based supercapacitor. *J. Power Sources* **2006**, *162*, 1460–1466. [[CrossRef](#)]
12. Ramachandran, R.; Wang, F. Electrochemical Capacitor Performance: Influence of Aqueous Electrolytes. *Supercapacitors Theor. Pract. Solut.* **2017**. [[CrossRef](#)]
13. Pal, B.; Yang, S.; Ramesh, S.; Thangadurai, V.; Jose, R. Electrolyte selection for supercapacitive devices: A critical review. *Nanoscale Adv.* **2019**, *1*, 3807–3835. [[CrossRef](#)]
14. Dyatkin, B.; Mamontov, E.; Cook, K.M.; Gogotsi, Y. Capacitance, charge dynamics, and electrolyte-surface interactions in functionalized carbide-derived carbon electrodes. *Prog. Nat. Sci.* **2015**, *25*, 631–641. [[CrossRef](#)]
15. Käärik, M.; Arulepp, M.; Kook, M.; Mäeorg, U.; Kozlova, J.; Sammelselg, V.; Perkson, A.; Leis, J. Characterisation of steam-treated nanoporous carbide-derived carbon of TiC origin: Structure and enhanced electrochemical performance. *J. Porous Mater.* **2017**, *25*, 1057–1070. [[CrossRef](#)]
16. Käärik, M.; Arulepp, M.; Kook, M.; Kozlova, J.; Ritslaid, P.; Aruväli, J.; Mäeorg, U.; Sammelselg, V.; Leis, J. High-performance microporous carbon from deciduous wood-origin metal carbide. *Microporous Mesoporous Mater.* **2019**, *278*, 14–22. [[CrossRef](#)]
17. Lota, K.; Sierczynska, A.; Acznik, I. Effect of aqueous electrolytes on electrochemical capacitor capacitance. *Chemik* **2013**, *67*, 1138–1145.
18. Barzegar, F.; Momodu, D.Y.; Fashedemi, O.O.; Bello, A.; Dangbegnon, J.K.; Manyala, N. Investigation of different aqueous electrolytes on the electrochemical performance of activated carbon-based supercapacitors. *RSC Adv.* **2015**, *5*, 107482–107487. [[CrossRef](#)]
19. Ibukun, O.; Jeong, H.K. Effects of Aqueous Electrolytes in Supercapacitors. *New Phys. Sae Mulli* **2019**, *69*, 154–158. [[CrossRef](#)]
20. Lang, A.W.; Ponder, J.F.; Österholm, A.M.; Kennard, N.J.; Bulloch, R.H.; Reynolds, J.R. Flexible, aqueous-electrolyte supercapacitors based on water-processable dioxothiophene polymer/carbon nanotube textile electrodes. *J. Mater. Chem. A* **2017**, *5*, 23887–23897. [[CrossRef](#)]
21. Mao, X.; Hatton, T.A.; Rutledge, G.C. A Review of Electrospun Carbon Fibers as Electrode Materials for Energy Storage. *Curr. Org. Chem.* **2013**, *17*, 1390–1401. [[CrossRef](#)]
22. Frackowiak, E.; Abbas, Q.; Béguin, F. Carbon/carbon supercapacitors. *J. Energy Chem.* **2013**, *22*, 226–240. [[CrossRef](#)]
23. Ruiz, V.; Santamaría, R.; Granda, M.; Blanco, C. Long-term cycling of carbon-based supercapacitors in aqueous media. *Electrochim. Acta* **2009**, *54*, 4481–4486. [[CrossRef](#)]
24. Khomenko, V.; Raymundo-Piñero, E.; Béguin, F. A new type of high energy asymmetric capacitor with nanoporous carbon electrodes in aqueous electrolyte. *J. Power Sources* **2010**, *195*, 4234–4241. [[CrossRef](#)]
25. Demarconnay, L.; Raymundo-Piñero, E.; Béguin, F. A symmetric carbon/carbon supercapacitor operating at 1.6V by using a neutral aqueous solution. *Electrochem. Commun.* **2010**, *12*, 1275–1278. [[CrossRef](#)]
26. Béguin, F.; Presser, V.; Balducci, A.; Frackowiak, E. Carbons and Electrolytes for Advanced Supercapacitors. *Adv. Mater.* **2014**, *26*, 2219–2251. [[CrossRef](#)] [[PubMed](#)]
27. Cai, Y.-M.; Qin, Z.-Y.; Chen, L. Effect of electrolytes on electrochemical properties of graphene sheet covered with polypyrrole thin layer. *Prog. Nat. Sci.* **2011**, *21*, 460–466. [[CrossRef](#)]
28. Xu, C.; Wei, C.; Li, B.; Kang, F.; Guan, Z. Charge storage mechanism of manganese dioxide for capacitor application: Effect of the mild electrolytes containing alkaline and alkaline-earth metal cations. *J. Power Sources* **2011**, *196*, 7854–7859. [[CrossRef](#)]
29. Jenkins, H.D.B.; Thakur, K.P. Reappraisal of thermochemical radii for complex ions. *J. Chem. Educ.* **1979**, *56*, 576. [[CrossRef](#)]
30. Park, J.-S. Electrospinning and its applications. *Adv. Nat. Sci. Nanosci. Nanotechnol.* **2010**, *1*, 043002. [[CrossRef](#)]
31. Sundarrajan, S.; Tan, K.L.; Lim, S.H.; Ramakrishna, S. Electrospun Nanofibers for Air Filtration Applications. *Procedia Eng.* **2014**, *75*, 159–163. [[CrossRef](#)]
32. Rahman, M.M.; Tahkar, A.I. Use of Nano Fibers in Filtration—A review. *IJSRD-Int. J. Sci. Res. Dev.* **2016**, *4*, 7.
33. Ding, B.; Wang, M.; Wang, X.; Yu, J.; Sun, G. Electrospun nanomaterials for ultrasensitive sensors. *Mater. Today* **2010**, *13*, 16–27. [[CrossRef](#)]

34. Sun, G.; Sun, L.; Xie, H.; Liu, J. Electrospinning of Nanofibers for Energy Applications. *Nanomaterials* **2016**, *6*, 129. [[CrossRef](#)] [[PubMed](#)]
35. Li, X.; Zhao, Y.; Bai, Y.; Zhao, X.; Wang, R.; Huang, Y.; Liang, Q.; Huang, Z. A Non-Woven Network of Porous Nitrogen-doping Carbon Nanofibers as a Binder-free Electrode for Supercapacitors. *Electrochim. Acta* **2017**, *230*, 445–453. [[CrossRef](#)]
36. He, T.; Fu, Y.; Meng, X.; Yu, X.; Wang, X. A novel strategy for the high performance supercapacitor based on polyacrylonitrile-derived porous nanofibers as electrode and separator in ionic liquid electrolyte. *Electrochim. Acta* **2018**, *282*, 97–104. [[CrossRef](#)]
37. Tönurist, K.; Vaas, I.; Thomberg, T.; Jänes, A.; Kurig, H.; Romann, T.; Lust, E. Application of multistep electrospinning method for preparation of electrical double-layer capacitor half-cells. *Electrochim. Acta* **2014**, *119*, 72–77. [[CrossRef](#)]
38. Malmberg, S.; Tarasova, E.; Vassiljeva, V.; Krasnou, I.; Arulepp, M.; Krumme, A. *Fully Electrospun Durable Electrode and Electrochemical Double-Layer Capacitor for High Frequency Applications*; ESA SPCD: Lanskröun, Czech Republic, 2018; p. 10.
39. Malmberg, S.; Arulepp, M.; Savest, N.; Tarasova, E.; Vassiljeva, V.; Krasnou, I.; Käärik, M.; Mikli, V.; Krumme, A.; Malmberg, S. Directly electrospun electrodes for electrical double-layer capacitors from carbide-derived carbon. *J. Electroanal. Chem.* **2020**, *103*, 103396. [[CrossRef](#)]
40. Malmberg, S.; Arulepp, M.; Tarasova, E.; Vassiljeva, V.; Krasnou, I.; Krumme, A. Electrochemical Evaluation of Directly Electrospun Carbide-Derived Carbon-Based Electrodes in Different Nonaqueous Electrolytes for Energy Storage Applications. *C. J. Carbon Res.* **2020**, *6*, 59. [[CrossRef](#)]
41. Balbuena, P.B. Electrolyte Materials-Issues and Challenges. In Proceedings of the AIP Conference Proceedings, Freiberg, Germany, 17 February 2014; pp. 82–97. [[CrossRef](#)]
42. Conway, B.E. Behavior of the Double Layer in Nonaqueous Electrolytes and Nonaqueous Electrolyte Capacitors. In *Electrochemical Supercapacitors*; Springer: Boston, MA, USA, 1999; pp. 169–181.
43. Balducci, A. Electrolytes for high voltage electrochemical double layer capacitors: A perspective article. *J. Power Sources* **2016**, *326*, 534–554. [[CrossRef](#)]
44. Tomiyasu, H.; Shikata, H.; Takao, K.; Asanuma, N.; Taruta, S.; Park, Y.-Y. An aqueous electrolyte of the widest potential window and its superior capability for capacitors. *Sci. Rep.* **2017**, *7*, srep45048. [[CrossRef](#)]
45. Bu, X.; Su, L.; Dou, Q.; Lei, S.; Yan, X. A low-cost “water-in-salt” electrolyte for a 2.3 V high-rate carbon-based supercapacitor. *J. Mater. Chem. A* **2019**, *7*, 7541–7547. [[CrossRef](#)]
46. Lee, M.H.; Kim, S.J.; Chang, D.; Kim, J.; Moon, S.; Oh, K.; Park, K.-Y.; Seong, W.M.; Park, H.; Kwon, G.; et al. Toward a low-cost high-voltage sodium aqueous rechargeable battery. *Mater. Today* **2019**, *29*, 26–36. [[CrossRef](#)]
47. Stojanovska, E.; Pampal, E.S.; Kilic, A.; Quddus, M.; Candan, Z. Developing and characterization of lignin-based fibrous nanocarbon electrodes for energy storage devices. *Compos. Part B Eng.* **2019**, *158*, 239–248. [[CrossRef](#)]
48. Khosrozadeh, A.; Singh, G.; Wang, Q.; Luo, G.; Xing, M. Supercapacitor with extraordinary cycling stability and high rate from nano-architected polyaniline/graphene on Janus nanofibrous film with shape memory. *J. Mater. Chem. A* **2018**, *6*, 21064–21077. [[CrossRef](#)]
49. Jia, Z.; Liu, D.Q.; Yang, S.Y. Electrochemical Insight into Cycle Stability of Organic Electrolyte Supercapacitors. *Adv. Mater. Res.* **2011**, *347–353*, 467–471. [[CrossRef](#)]
50. Brunauer, S.; Emmett, P.H.; Teller, E. Adsorption of Gases in Multimolecular Layers. *J. Am. Chem. Soc.* **1938**, *60*, 309–319. [[CrossRef](#)]
51. Thommes, M.; Kaneko, K.; Neimark, A.V.; Olivier, J.P.; Rodriguez-Reinoso, F.; Rouquerol, J.; Sing, K.S. Physisorption of gases, with special reference to the evaluation of surface area and pore size distribution (IUPAC Technical Report). *Pure Appl. Chem.* **2015**, *87*, 1051–1069. [[CrossRef](#)]
52. Lee, S.; Kim, J.; Ku, B.-C.; Kim, J.; Joh, H.-I. Structural Evolution of Polyacrylonitrile Fibers in Stabilization and Carbonization. *Adv. Chem. Eng. Sci.* **2012**, *2*, 275–282. [[CrossRef](#)]
53. Li, J.; Su, S.; Zhou, L.; Kunderát, V.; Abbot, A.M.; Mushtaq, F.; Ouyang, D.; James, D.; Roberts, D.; Ye, H. Carbon nanowalls grown by microwave plasma enhanced chemical vapor deposition during the carbonization of polyacrylonitrile fibers. *J. Appl. Phys.* **2013**, *113*, 024313. [[CrossRef](#)]
54. Surianarayanan, M.; Vijayaraghavan, R.; Raghavan, K.V. Spectroscopic investigations of polyacrylonitrile thermal degradation. *J. Polym. Sci. Part Polym. Chem.* **1998**, *36*, 2503–2512. [[CrossRef](#)]
55. Conley, R.T.; Bieron, J.F. Examination of the oxidative degradation of polyacrylonitrile using infrared spectroscopy. *J. Appl. Polym. Sci.* **1963**, *7*, 1757–1773. [[CrossRef](#)]
56. Henrici-Olivé, G.; Olivé, S. Molecular interactions and macroscopic properties of polyacrylonitrile and model substances. In *Chemistry*; Springer: Berlin/Heidelberg, Germany, 1979; Volume 32, pp. 123–152. [[CrossRef](#)]
57. Torop, J.; Palmre, V.; Arulepp, M.; Sugino, T.; Asaka, K.; Aabloo, A. Flexible supercapacitor-like actuator with carbide-derived carbon electrodes. *Carbon* **2011**, *49*, 3113–3119. [[CrossRef](#)]
58. Barsoukov, E.; Macdonald, J.R. (Eds.) *Impedance Spectroscopy: Theory, Experiment, and Applications*, 2nd ed.; Wiley-Interscience: Hoboken, NJ, USA, 2005.

-
59. Feng, X. *Nanocarbons for Advanced Energy Storage, Volume 1*; John Wiley & Sons: Hoboken, NJ, USA, 2015.
 60. Fic, K.; Lota, G.; Meller, M.; Frackowiak, E. Novel insight into neutral medium as electrolyte for high-voltage supercapacitors. *Energy Environ. Sci.* **2012**, *5*, 5842–5850. [[CrossRef](#)]
 61. He, M.; Fic, K.; Frackowiak, E.; Novák, P.; Berg, E.J. Influence of aqueous electrolyte concentration on parasitic reactions in high-voltage electrochemical capacitors. *Energy Storage Mater.* **2016**, *5*, 111–115. [[CrossRef](#)]